

A FURTHER STUDY OF THE MOLECULAR CLOUD ASSOCIATED WITH THE SUPERNOVA REMNANT G109.1–1.0

KEN'ICHI TATEMATSU, YASUO FUKUI, AND TAKAHIRO IWATA

Department of Astrophysics, Nagoya University

FREDERICK D. SEWARD

Harvard-Smithsonian Center for Astrophysics

AND

MAKOTO NAKANO

Department of Earth Science, Faculty of Education, Oita University

Received 1989 May 8; accepted 1989 August 28

ABSTRACT

The region of the semicircular supernova remnant G109.1–1.0 (CTB 109) is studied on the basis of CO observations with the Nobeyama Radio Observatory (NRO) 45 m radio telescope and X-ray data from the archive of the *Einstein Observatory*. By observing the $J = 1-0$ transition of CO at 115 GHz, the distribution of the molecular cloud associated with the remnant is investigated in detail. The resolution of the CO mapping observations is $30''-60''$ (0.6–1.2 pc), and the number of the CO spectra obtained is about 2000. The molecular ridge (CO arm), which was known to show an apparent anticorrelation with the curled X-ray jetlike feature of the remnant, is resolved into two CO filaments. X-ray spectra toward the CO arm are harder than those toward the surrounding region. The harder X-ray spectrum, together with the decrease of the X-ray intensity, suggests that X-ray absorption takes place, although there remains a possibility that hotter plasma is located along the line of sight toward the CO arm by chance. The hardness of the X-ray spectrum toward the CO arm is consistent with the column densities of the two CO filaments. However, the overall appearance of the remnant will not be affected very much by the absorption, because the X-ray absorption is found to be a minor effect. Shock-accelerated CO gas has not been observed toward the G109.1–1.0 region. The upper bound to the intensity of shock-accelerated CO gas is 0.4 K for the whole mapped region, and the upper bound toward 11 points observed at a lower noise level is 0.1 K. These upper bounds are below the intensity (1–2 K) of shock-accelerated CO gas associated with IC 443.

Subject headings: interstellar: molecules — nebulae: individual (G109.1–1.0, CTB 109) — nebulae: supernova remnants — X-rays: sources — X-rays: spectra

I. INTRODUCTION

G109.1–1.0 (CTB 109) is a supernova remnant with a semi-circular shape (Gregory and Fahlman 1980; Downes 1983; Sofue, Takahara, and Hirabayashi 1983; Hughes *et al.* 1984). The X-ray pulsar 1E 2259+586 is located at the center of the remnant (Fahlman and Gregory 1981, 1983; Koyama, Hoshi, and Nagase 1987), and a curled X-ray jetlike feature extends from the X-ray pulsar to the remnant shell (Gregory and Fahlman 1980, 1981; see also Gregory and Fahlman 1983).

A giant molecular cloud in the direction of G109.1–1.0 has been observed in the $J = 1-0$ transitions of CO and/or ^{13}CO by several groups at $3'-8'$ resolution, and the association of G109.1–1.0 with this giant molecular cloud has been investigated (Israel 1980; Heydari-Malayeri, Kahane, and Lucas 1981; Gregory *et al.* 1983; Tatematsu *et al.* 1985, 1987). The $3'$ resolution observations by Tatematsu *et al.* (1987) have clearly shown that the western chord of the semicircular shape of G109.1–1.0 just corresponds to the eastern boundary of the main body of the giant molecular cloud. They also pointed out that a molecular ridge (CO arm), which extends from the main body of the cloud, shows an apparent anticorrelation with the curled X-ray jetlike feature of the remnant; the CO arm is apparently surrounded by the X-ray jetlike feature. Tatematsu *et al.* (1987) suggested that the absorption of the X-ray emission by the CO arm is responsible for the anticorrelation between them.

In this paper, we report detailed CO observations with the 45 m radio telescope of the Nobeyama Radio Observatory¹ (NRO) and examination of the archival X-ray data of G109.1–1.0 obtained with the *Einstein Observatory*. Except for the spectrum toward the X-ray pulsar, X-ray spectra of the *Einstein Observatory* toward this remnant have not been analyzed in detail. The purposes of the present study are (1) to know whether the X-ray absorption by the CO arm actually takes place or not, and (2) to search for dynamical influence of G109.1–1.0 on the molecular cloud. For the first purpose, we compare a high-resolution CO map with the X-ray image of the remnant to assess the anticorrelation between the CO arm and the X-ray jetlike feature, and we analyze the X-ray data to search for evidence of absorption. For the second purpose, we search for Doppler-shifted wing emission in CO spectra. Until now, IC 443 has remained a unique example which shows broad molecular emission indicating shocks (DeNoyer 1979; DeNoyer and Frerking 1981; Huang, Dickman, and Snell 1986; White *et al.* 1987). Since we know that G109.1–1.0 is associated with the molecular cloud, a search for broad CO emission is of interest. Throughout this paper, the distance to this region is assumed to be 4.0 kpc (see Tatematsu *et al.* 1987, and references therein). In § II, we describe the CO observa-

¹ The Nobeyama Radio Observatory is a branch of the National Astronomical Observatory, an interuniversity research institute operated by the Ministry of Education, Science, and Culture, Japan.

tions and the X-ray data. The distribution of the molecular cloud and the negative result of a search for shock-accelerated CO gas are presented in § III. In § IV, we examine the X-ray spectra of the remnant and estimate the absorbing column density corresponding to the molecular cloud. Evidence of X-ray absorption, the true X-ray image of G109.1–1.0, and the meaning of the lack of shock-accelerated CO gases in this region are discussed in § V.

II. OBSERVATIONS

a) CO Observations

Observations were carried out in the $J = 1-0$ transition of the CO ($^{12}\text{C}^{16}\text{O}$) molecule at 115 GHz by using the NRO 45 m radio telescope in three periods: 1986 December, 1987 April, and 1987 December. This radio telescope has a half-power beamwidth of $17'' \pm 1''$ and a beam efficiency of 0.45 ± 0.05 at this frequency. A cooled Schottky mixer receiver was employed, and it provided a system temperature of 700–1000 K (SSB). We used one of the acousto-optical spectrometers having 37 kHz (0.1 km s^{-1}) resolution. Pointing of the telescope was established by observing one of the relevant SiO maser sources at 43 GHz every 2 hr at least, and its accuracy was typically $5''-10''$. We have mapped an area covering the remnant at spacings of $30''-60''$, and ~ 2000 spectra were obtained. The observed area and spacing intervals are illustrated in Figure 1. The typical rms noise level is $0.35-0.4 \text{ K}$ for the mapping observations, when the spectra are smoothed to 360 kHz (0.9 km s^{-1}) resolution. To investigate the existence of shock-accelerated CO gas, we observed the 11 additional points listed in Table 1 at lower noise levels. All the spectra were obtained in the position switching mode, and only linear baselines were subtracted from them. The flatnesses of the baselines are sufficient for a search for broad CO emission. The line intensity was calibrated by using the standard chopper-wheel method and is expressed in terms of the corrected antenna temperature T_A^* (Kutner and Ulich 1981, and references therein).

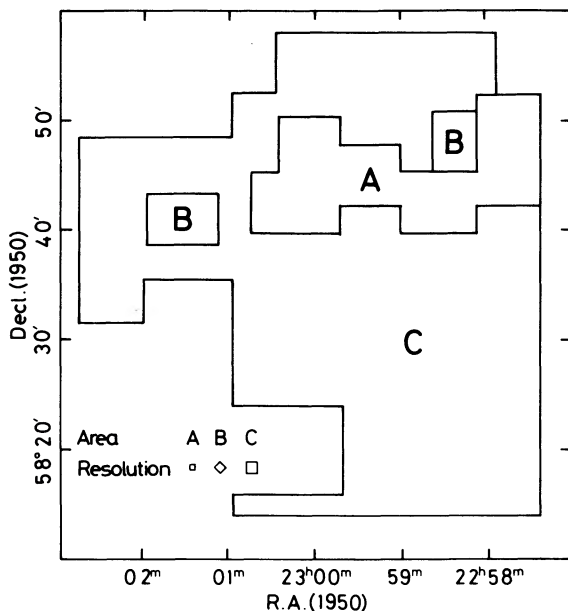


FIG. 1.—Area observed in CO ($J = 1-0$). A, B, and C denote regions observed at spacing intervals of $30''$, $42.4''$, and $60''$, respectively.

TABLE 1
POINTS OBSERVED AT LOWER NOISE LEVELS

R.A.(1950)	Decl.(1950)	rms Noise Level*	Comment
22 ^h 57 ^m 44 ^s .6	58°36'30"	0.10 K	Not used for map
22 57 48.5	58 36 30	0.10 K	Not used for map
22 57 52.3	58 36 30	0.10 K	Not used for map
22 57 56.2	58 36 30	0.10 K	Not used for map
22 58 00.0	58 36 30	0.10 K	Not used for map
22 58 43.3	58 43 30	0.15 K	...
22 58 43.3	58 44 30	0.15 K	...
23 01 36.6	58 40 30	0.12 K	...
23 01 40.4	58 40 30	0.12 K	...
23 01 44.3	58 40 30	0.12 K	...
23 01 48.1	58 40 30	0.12 K	...

* At 360 kHz resolution.

b) X-Ray Observations

We extracted the data of G109.1–1.0, which have been obtained with the Imaging Proportional Counter (IPC) on board the *Einstein Observatory*, from the archive at the Harvard-Smithsonian Center for Astrophysics. Details of the *Einstein Observatory* are given in Giacconi *et al.* (1979). These data were originally obtained by Gregory and Fahlman (1980) and Fahlman and Gregory (1983) as four separate observations (I8102, 19984, 19985, and 19986). An observation log is given in Fahlman and Gregory (1983). They have analyzed a spectrum toward the X-ray pulsar, but X-ray spectra of the remnant, excluding the X-ray pulsar, have not been investigated in detail. We use the same X-ray data to search for X-ray absorption by the CO arm. We analyzed the data I8102 separately from 19984, 19985, and 19986, because there was a large temporal change in the detector gain between these fields. We merged the data 19984, 19985, and 19986 to make one data set. The photon counts in PH (pulse height) channels 4–9, which correspond to 0.63–3.05 keV in I8102 and to 0.45–2.21 keV in 19984–19986, were used for spectral analysis. We omitted the counts in PH channels 1–3 and 10–15 in spectral fitting, because in these channels the number of source counts is small and also because the instrumental spatial resolution becomes larger (> 2.2 FWHM) in channels 1–3. The X-ray image of G109.1–1.0, background subtracted and corrected for vignetting, was constructed by adding all four data fields.

III. RESULTS OF THE CO OBSERVATIONS

a) CO Distribution

Figure 2 is a contour map of the CO intensity integrated from -57 to -43 km s^{-1} in V_{LSR} . Most of the CO profiles range from -53 to -47 km s^{-1} , and a map of the CO intensity integrated within this narrower range is shown in Figure 3. Thin lines in Figure 3 represent a 0.5–4.5 keV X-ray map of G109.1–1.0. The X-ray map, which was convolved with a Gaussian function of width $\sigma = 32''$, has a resolution of $\sim 2'$ FWHM. On the X-ray map, the X-ray pulsar 1E 2259+586 is located at the center of the remnant, and the curled X-ray jetlike feature extends eastward from it. The CO emission seen on the right side of these maps is an eastern part of the main molecular cloud (see, e.g., Tatematsu *et al.* 1985 for its overall structure). This outer part of the main molecular cloud appears conspicuously clumpy. The CO intensity is not intense ($2-6 \text{ K km s}^{-1}$) near the boundary of the main molecular cloud, and there is no enhancement in CO intensity along the interface with G109.1–1.0.

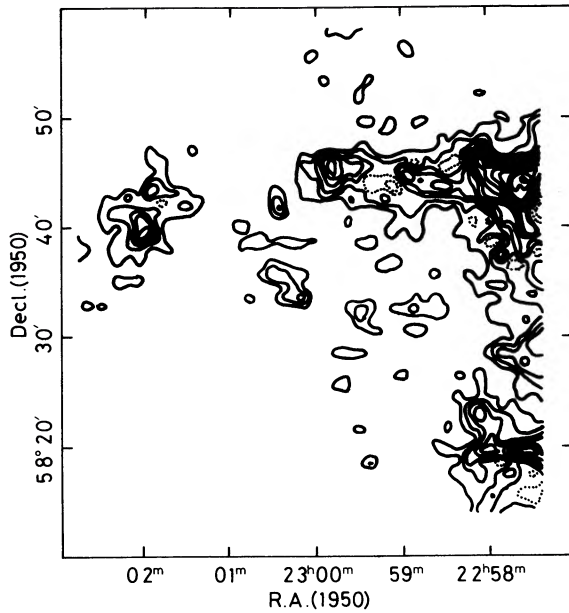


FIG. 2.—Contour map of the CO ($J=1-0$) intensity integrated over the radial velocity range $V_{\text{LSR}} = (-57, -43)$ km s^{-1} . Contour interval is 3 K km s^{-1} .

The CO arm extending along $\text{Decl. (1950)} = 58^\circ 45'$, which was previously recognized as one ridge, is resolved into two CO filaments. These two CO filaments have different peak velocities of -50 km s^{-1} and -48 km s^{-1} , respectively, and are shown separately in two equi-velocity maps (Figs. 4 and 5). Five CO spectra taken along $\text{R.A.} = 22^{\text{h}}59^{\text{m}}06^{\text{s}}.4$ (Fig. 6) clearly illustrate the velocity difference of the two filaments, from -50 km s^{-1} to -48 km s^{-1} in V_{LSR} . Figure 4 represents

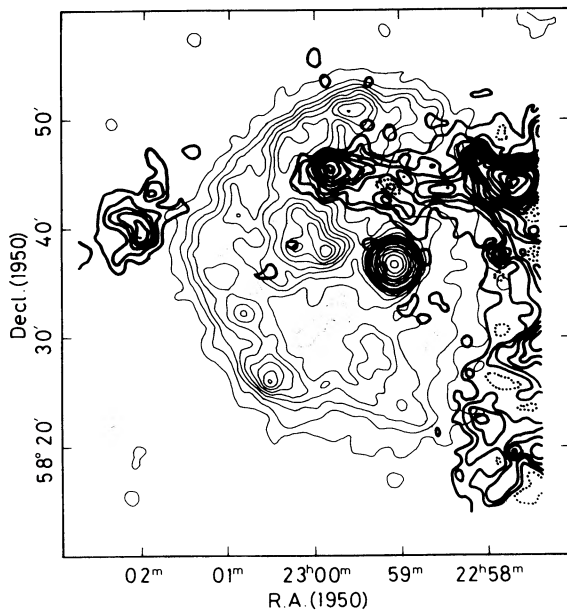


FIG. 3.—Map of the CO intensity integrated over $V_{\text{LSR}} = (-53, -47)$ km s^{-1} is shown as thick lines. The 0.5–4.5 keV X-ray map of G109.1-1.0 obtained with the *Einstein Observatory* is superposed as thin lines. Contour interval for the CO emission is 2.3 K km s^{-1} . Contours of the X-ray emission are drawn at (7.9, 24, 39, 55, 71, 87, 103, 118, 134, 150, 166, 234, 331, 467, 660, 932, 1316, 1859) $\times 10^{-4}$ IPC counts $\text{s}^{-1} \text{ arcmin}^{-2}$. Resolution of the X-ray map is $\sim 2'$ FWHM.

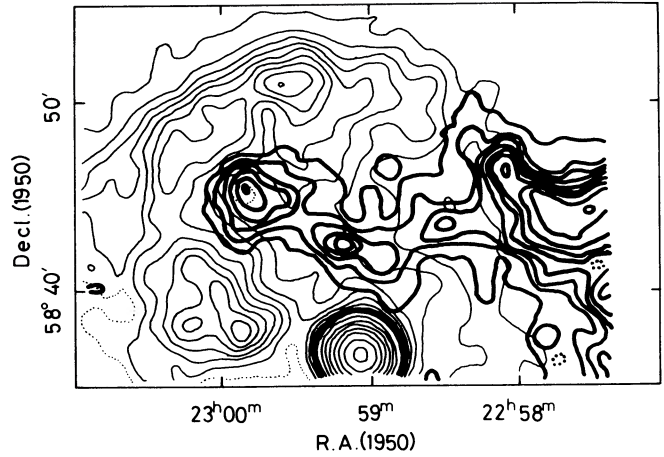


FIG. 4.—Map of the CO emission at the radial velocity interval $V_{\text{LSR}} = (-51, -49)$ km s^{-1} toward the CO arm (thick lines). Contour interval is 1.5 K km s^{-1} . The X-ray map is superposed as thin lines.

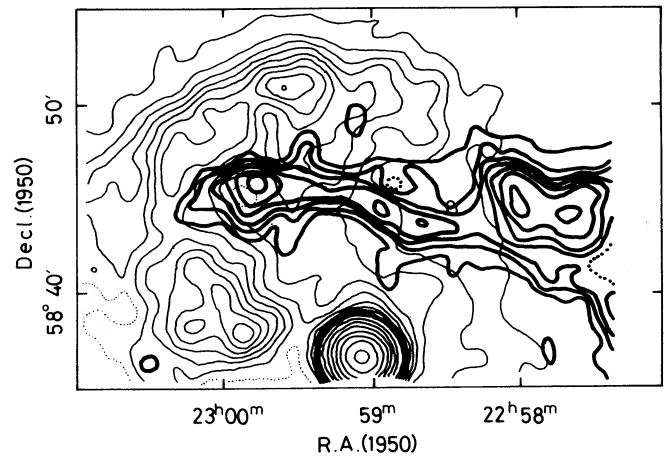


FIG. 5.—Same as Fig. 4, but for $V_{\text{LSR}} = (-49, -47)$ km s^{-1}

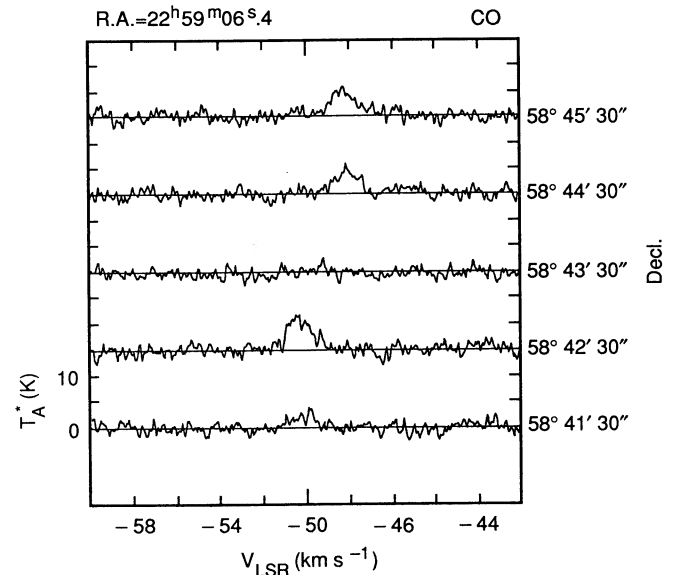


FIG. 6.—Examples of the CO profiles observed toward the CO arm

the CO intensity integrated at the velocity interval $V_{\text{LSR}} = (-51, -49) \text{ km s}^{-1}$, and Figure 5 represents the intensity at the interval $V_{\text{LSR}} = (-49, -47) \text{ km s}^{-1}$. The southern CO filament has a curled shape (Fig. 4), whereas the northern CO filament has a rather straight shape (Fig. 5). The west part of the northern CO filament [R.A.(1950) = $22^{\text{h}}58^{\text{m}}20^{\text{s}}-59^{\text{m}}00^{\text{s}}$] is observed over the range $V_{\text{LSR}} = (-49, -45) \text{ km s}^{-1}$. The extents of these two CO filaments are $2'-3'$ (2–3 pc) in width and $\sim 14'$ (16 pc) in length. The two CO filaments extend from the common root [R.A.(1950) = $22^{\text{h}}58^{\text{m}}20^{\text{s}}-58^{\text{m}}40^{\text{s}}$, decl.(1950) = $58^{\circ}44'$] to the common top, a CO peak [R.A.(1950) = $22^{\text{h}}59^{\text{m}}50^{\text{s}}$, decl.(1950) = $58^{\circ}45'$]. Since the two filaments extend from the main molecular cloud, which is associated with G109.1–1.0, they are thought to be located within or just near this supernova remnant. These CO filaments are surrounded by a curled X-ray ridge or the X-ray jetlike feature (see the fifth contour of X-rays in Fig. 3) as pointed out by Tatematsu *et al.* (1987). In particular, the CO peak is located just toward a relative depression of the X-ray intensity centered on R.A. = $22^{\text{h}}59^{\text{m}}9$, decl. = $58^{\circ}45'$ with a diameter of $4'$, and the root part of the CO filaments is located toward a relative depression at R.A. = $22^{\text{h}}58^{\text{m}}4-59^{\text{m}}0$, decl. = $58^{\circ}42'-47'$. The anticorrelation is generally good except for the point R.A.(1950) = $22^{\text{h}}59^{\text{m}}4$, decl.(1950) = $58^{\circ}41'$, where both the X-ray and CO emission are weak (see also Fig. 2 of Tatematsu *et al.* 1987).

To obtain the column densities and masses of the two CO filaments, we use the CO and ^{13}CO data obtained with the Nagoya 4 m radio telescope (Tatematsu *et al.* 1987). Although their integrated CO map (see their Fig. 2) does not resolve the CO arm into the two filaments, radial velocity of the ^{13}CO emission helps us to identify which part of the CO arm on the 4 m telescope data corresponds to either of the two filaments. The northern half of the CO arm on the 4 m telescope data shows the ^{13}CO emission at a radial velocity of -48 km s^{-1} , whereas the southern half shows the emission at -50 km s^{-1} velocity. We have selected three observed positions for the northern filament and one position for the southern filament to obtain the representative values of the column densities of the CO filaments. The H_2 column densities toward the northern and southern CO filaments are estimated to be $8-10 \times 10^{20} \text{ cm}^{-2}$ and $\sim 2 \times 10^{20} \text{ cm}^{-2}$, respectively. Here we adopt the standard method assuming local thermodynamic equilibrium (LTE) to estimate the ^{13}CO column density, and we convert it to the H_2 column density by multiplying by 5×10^5 (Dickman 1978). The common root part of the two CO filaments has almost the same H_2 column density as the northern CO filament. The CO peak has an H_2 column density of $2 \times 10^{21} \text{ cm}^{-2}$. The average H_2 number densities in the northern and southern CO filaments are estimated to be $100-150 \text{ cm}^{-3}$ and 30 cm^{-3} , respectively. We assume now that both the CO filaments have a depth along the line of sight of 2–3 pc, which is the same value as the width of the filaments as resolved with the 45 m radio telescope. The H_2 density of 30 cm^{-3} estimated for the southern CO filament is lower than the value $\gtrsim 10^2 \text{ cm}^{-3}$. This value may be lower than that needed to collisionally excite the $J = 1-0$ transition, even when radiation trapping is taken into account. The density in the southern filament might be underestimated; e.g., the true depth may be smaller than the assumed value, or the filling factor of CO emitting gas for the 4 m telescope beam may be smaller than unity. The diffuse parts of the northern and southern CO filaments, excluding the CO peak, have a length of 12 pc, and their masses are estimated to be $500-700 M_{\odot}$ and $100-150 M_{\odot}$,

respectively. The CO peak has a mass of $900 M_{\odot}$ within the half-intensity contour of the column density map (4.5 or 5.2 pc in diameter), and the average H_2 density is estimated to be 130 cm^{-3} by assuming that its shape is spherical. We adopt here a mean molecular weight per H_2 molecule of $2.76 m_{\text{H}}$ for mass estimation. The values quoted here are lower limits, because gases in atomic form are not included.

An eastern molecular cloud centered on R.A.(1950) = $23^{\text{h}}02^{\text{m}}$, decl.(1950) = $58^{\circ}40'$, which was first detected by Tatematsu *et al.* (1987), is thought to belong to the G109.1–1.0 region because it is located near the remnant shell and also because its radial velocity (-49 to -46 km s^{-1}) is close to those of the CO filaments. The velocity gradient in the EW direction reported by Tatematsu *et al.* (1987) is confirmed in the present, higher resolution study.

b) Search for Shock-Accelerated CO Gas

The CO spectra obtained in the CO mapping observations have line widths of a few km s^{-1} FWHM in general. Such narrow CO emission probably comes from unperturbed gases. Only toward a molecular clump centered on R.A.(1950) = $22^{\text{h}}57^{\text{m}}7$, decl.(1950) = $58^{\circ}43'$ did we obtain relatively broad CO spectra having line widths of $4-7 \text{ km s}^{-1}$ FWHM, but the line shape and line width of the CO spectra are typical of the dense part of the giant molecular cloud rather than indicative of shock-accelerated CO gas (see Tatematsu *et al.* 1985). The velocity difference of 2 km s^{-1} between the northern and southern CO filaments are too small to be attributed to the dynamical influence of G109.1–1.0. The rms noise level for the whole mapped region is typically $0.35-0.4 \text{ K}$ at 360 kHz (0.9 km s^{-1}) resolution.

To obtain a better constraint, we observed 11 additionally selected points (Table 1) at lower noise levels. We selected positions near the edge of the molecular cloud which seem to have been struck by the supernova remnant; four points were selected on the eastern molecular cloud and five points were selected near the edge of the main molecular cloud. We also observed two points at the root part of the CO filaments. Figure 7 shows CO spectra smoothed to 360 kHz (0.9 km s^{-1}) resolution. The rms noise level toward the 11 selected points is $0.1-0.15 \text{ K}$. The baselines of the obtained spectra are sufficiently flat. None of the spectra show any indication of broad-line emission.

Shock-accelerated CO gas is absent in the G109.1–1.0 region in the present CO study. The 3σ upper limit to the intensity of shock-accelerated CO gas, which is expected to have a line width of $>10 \text{ km s}^{-1}$ (4 MHz), is $\sim 0.4 \text{ K}$ for the whole mapped area and $\sim 0.1 \text{ K}$ toward the selected 11 points. These values are smaller than the CO intensity ($T_A^* = 1-2 \text{ K}$) of the gas accelerated by IC 443 (Huang, Dickman, and Snell 1986). The beam size and spacing intervals employed here are comparable in a projected linear dimension (parsecs) to those used in a survey of broad CO emission in IC 443 by Huang, Dickman, and Snell. It seems that the CO cloud associated with the supernova remnant does not necessarily mean the existence of shock-accelerated CO gases.

IV. EXAMINATION OF THE X-RAY SPECTRA

The purpose of the analysis was to search for the absorption of X-rays by the CO arm as suggested by Tatematsu *et al.* (1987). The X-ray spectra were extracted from six areas (Table 2 and Fig. 8). The observed X-ray spectrum, which has been only background subtracted, is harder toward the CO arm than in the cloud-free directions (not shown).

TABLE 2
AREAS FOR X-RAY SPECTRAL ANALYSIS

Area	R.A.(1950)	Decl.(1950)	Diameter	Comment
P1	22 ^h 59 ^m 42 ^s	58°45'0"	6'00"	...
P2	22 59 58	58 38.9	6 00	...
P3	23 00 35	58 46.7	6 00	...
P4	22 59 40	58 51.3	6 00	...
Q1	22 58 37	58 44.2	6 00	...
Q2	22 58 53	58 50.5	6 00	...
Background	22 57 08	58 36.8	10 40	I8102
Background	23 02 24	58 36.4	10 40	I9984, I9985, I9986

The harder X-ray spectrum may imply either hotter temperature or larger absorbing column density. Spectral fitting was performed by using the usual method of reduction for the IPC data (e.g., Leahy *et al.* 1985). The X-ray spectra background subtracted were fitted to model spectra convolved with the detector response; the model spectrum was the optically thin thermal spectrum of Raymond and Smith (1977) with absorbing column density. The data quality is not sufficient to give meaningful results by varying both temperature and column density as free parameters, because the effects of these two parameters are highly coupled. The molecular cloud (CO arm) corresponds to a local minimum in X-ray surface brightness, and fitting with a fixed temperature would be helpful to know whether the CO arm absorbs X-rays or not.

First, we fitted the X-ray spectra fixing the temperature at $kT = 0.9$ keV. The value 0.9 keV was determined by the results

of two-parameter fitting and by the restriction that the H column densities in the cloud free directions (P2-4, Q2) be consistent with an upper limit of $5 \times 10^{21} \text{ cm}^{-2}$ estimated from the optical reddening of stars in this region (Crampton, Georgelin, and Georgelin 1978; Gregory and Fahlman 1980). The results of fitting are shown in Figure 9. The column density was estimated by minimizing the χ^2 value. The 68% and 90% confidence levels are generated at $\chi_{\text{min}}^2 + 1$ and $\chi_{\text{min}}^2 + 2.7$, respectively (e.g., Lampton, Margon, and Bowyer 1976). The derived H column density is larger toward the CO arm. We also fitted the observed X-ray spectra at several fixed temperatures other than 0.9 keV. When the X-ray spectra were fitted by fixing temperature at $kT = 0.7, 1.1,$ and 1.3 keV, we also obtained the same tendency in absorbing column density (not shown). When $kT \leq 0.5$ keV or $kT \geq 1.5$ keV, the χ^2 values were too large to accept.

Next, by fixing H column density at $3.5 \times 10^{21} \text{ cm}^{-2}$, we fitted the observed spectra. The excess of temperature toward the CO arm was estimated to be 0.2 keV. This value is not very large, and the harder spectrum can be attributed to temperature variation over the remnant. In this case, the harder spectrum toward the CO arm is interpreted as chance coincidence: since dense interstellar gases tend to decrease the tem-

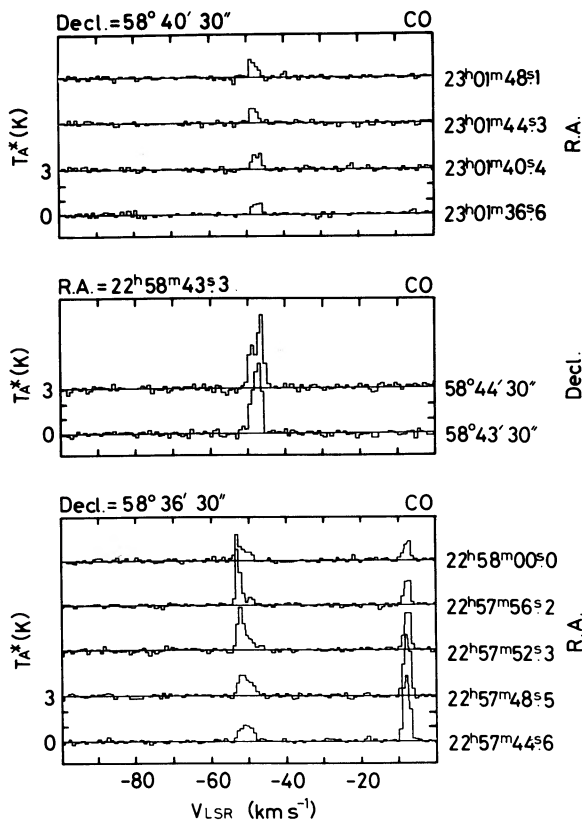


FIG. 7.—CO profiles obtained at lower noise levels. Spectra are smoothed to 360 kHz (0.9 km s^{-1}) resolution for showing flatness of the baseline well. The CO emission at $V_{\text{LSR}} = -8 \text{ km s}^{-1}$ represents a local molecular cloud.

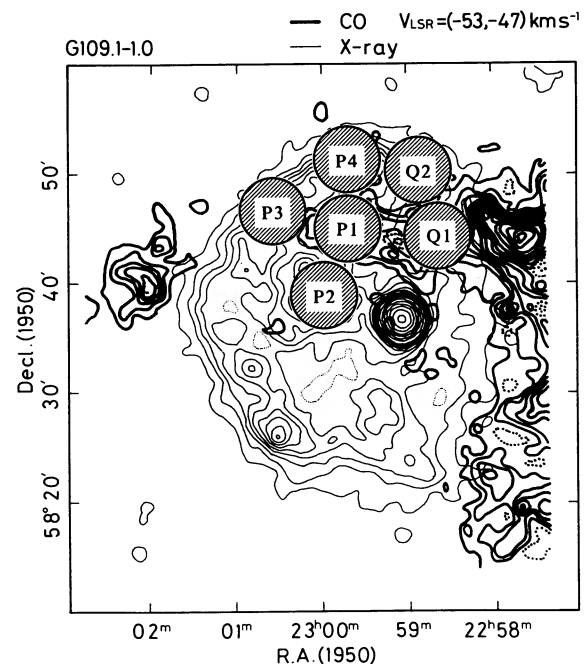


FIG. 8.—Areas used for X-ray spectral fitting

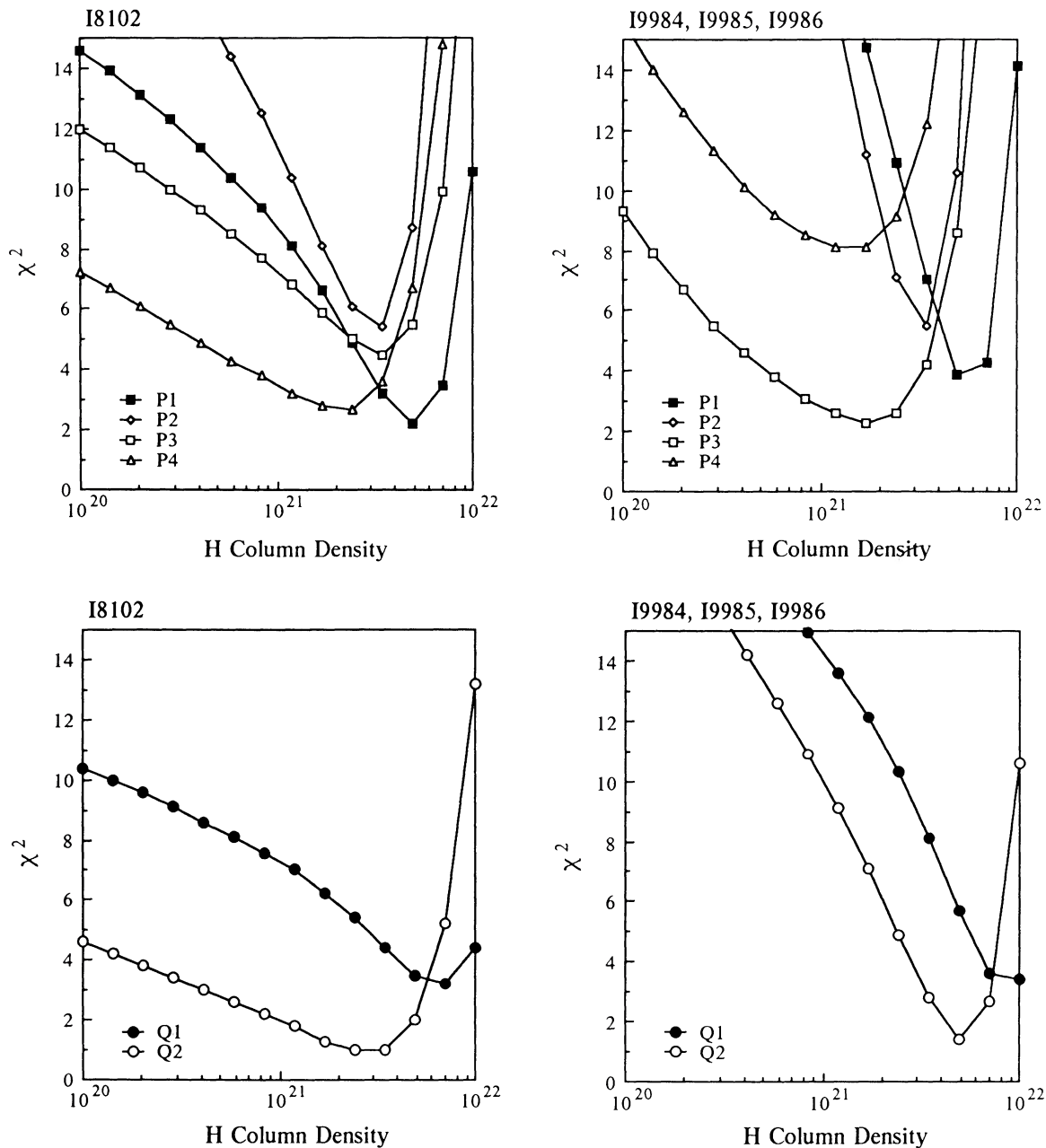


FIG. 9.—Results of the X-ray spectral fitting. The spectrum of the thermal plasma of Raymond and Smith (1977) at $kT = 0.9$ keV is assumed. H column density is estimated by minimizing the χ^2 value, and 90% confidence level is generated at $\chi_{\min}^2 + 2.7$ (Lampton, Margon, and Bowyer 1976). The data set I8102 (left panels) and the data set combining 19984, 19985, and 19986 (right panels) are processed independently, avoiding the influence of temporal variation of the detector gain.

perature of adjacent gases, hotter plasma cannot be physically related to the CO arm. We do not exclude the possibility of temperature variation, but the absorption model seems much more plausible when we take into account the anticorrelation of X-ray surface brightness with the CO distribution.

V. DISCUSSION

a) Evidence for X-Ray Absorption and the True X-Ray Image of the Remnant

We found an excess of absorbing column density toward the CO arm through spectral fitting at fixed temperature. The present results of the spectral fitting are thought to be reliable, because the independent data showed the same tendency: the

column density toward the CO arm (P1 and Q1) is consistently larger than that in the cloud-free direction (P2–4 and Q2) in all the four panels when we adopt the best-fit values (Fig. 9). The detector-gain calibration and background subtraction seem satisfactory because we have obtained consistent results from I8102 and 19984–19986, although the IPC detector gain varied between these fields and different areas were used for background subtraction (see Table 2). Furthermore, the results do not depend much on the temperature assumed in fitting, because the spectral fitting at 0.7, 1.1, and 1.3 keV showed the same tendency as the fitting at 0.9 keV did. In Figure 9, the excesses of the H column density toward P1 and Q1 are $1\text{--}4 \times 10^{21} \text{ cm}^{-2}$ and $\gtrsim 4 \times 10^{21} \text{ cm}^{-2}$, respectively. These

values are compatible with the estimates of the H column densities toward the CO peak (P1) and the root part of the CO arm (Q1) of $4 \times 10^{21} \text{ cm}^{-2}$ and $2 \times 10^{21} \text{ cm}^{-2}$, respectively, from the CO/ ^{13}CO data of Tatematsu *et al.* (1987). (Now the column densities of molecules are expressed as the number of H atoms for comparing with the X-ray absorbing column density.)

We wonder how G109.1–1.0 would look if the X-ray emission were not absorbed by the molecular cloud at all. Correction for the X-ray absorption by the CO arm will fill up the 4' diameter relative X-ray depression corresponding to the CO peak and the X-ray distribution like a “bay” corresponding to the root part of the CO arm. Absorption by the CO peak (H_2 column density = $2 \times 10^{21} \text{ cm}^{-2}$) and the root part ($1 \times 10^{21} \text{ cm}^{-2}$) may decrease the X-ray intensity by 47% and 29%, respectively. We assume here that there are foreground diffuse interstellar media having an H column density of $3 \times 10^{21} \text{ cm}^{-2}$ between the object and us. The decreases estimated here are upper bounds, because it is possible that the CO filaments are located within the remnant. Since the anticorrelation between the CO arm and the X-ray jetlike feature is not complete (§ IIIa), and the southern CO filament has a small column density, absorption will not explain the whole X-ray weak region surrounded by the X-ray jetlike feature. Whether the X-ray map is corrected for absorption or not, the X-ray blob at R.A.(1950) = $23^{\text{h}}00^{\text{m}}$, decl.(1950) = $58^{\circ}38'$, which is a part of the X-ray jetlike feature, is thought to be the most conspicuous feature next to the X-ray pulsar. It is likely that the observed X-ray map represents the true image of G109.1–1.0 basically, although the absorption by the CO arm has a minor effect on the X-ray map. The X-ray appearance of G109.1–1.0 will be mostly explained in terms of a combination of the X-ray pulsar, the semicircular X-ray shell structure, the additional X-ray blob, and the effect of X-ray absorption by the CO arm.

The origin of the additional X-ray blob must be discussed. Here we present two possible explanations. First, the X-ray blob might be related to the activity of the X-ray pulsar, because they are close to each other. Gregory and Fahlman (1980, 1981) proposed that the X-ray jetlike feature represents a jet ejected from the X-ray pulsar. This model is analogous to the X-ray jets observed toward the SS 433/W50 system (Seward *et al.* 1980; Watson *et al.* 1983). We are not sure whether the whole curled X-ray feature may represent a jet from the X-ray pulsar or not, because the curled X-ray feature (except for the conspicuous X-ray blob) cannot be discerned from the X-ray shell easily. The X-ray data do not show any trace of a counter blob, although there is no CO cloud absorbing X-rays. Thus, the blob is likely to be one-sided. The X-ray blob may represent an episodic ejection from the X-ray pulsar or gas illuminated by some kind of beam from the X-ray pulsar. Second, the X-ray blob may represent a local excess of the emission measure of postshock gases resulting from a density fluctuation in preshock gases. The X-ray intensity toward the X-ray blob is larger than in adjacent regions by a factor of 2–5. If the X-ray blob is spherical, its emissivity will be 5–20 times larger than the average value within the remnant. Since the emission measure is proportional to the square of electron density, a diffuse cloud having a somewhat (2–5 times) larger density than the average preshock density (of order 0.5 cm^{-3}) may have produced a feature like the X-ray blob after the passage of the blast wave. The density in the preexistent diffuse cloud would be less than several cm^{-3} , because the temperature of the gases in the X-ray blob must be greater than

10^6 K , to which the IPC detector is sensitive. If the diffuse cloud had been spatially located near the X-ray pulsar, it would be dispersed completely by now. Thus, in this model the X-ray blob should be located near the shell. One may attribute the origin of this preexistent cloud to a part of the tenuous skirts of the CO arm, because in general interstellar clouds have a density structure that decreases outward.

b) Lack of Shock-accelerated CO Gases and the Physical Condition of the Molecular Cloud

The results of the present CO observations give no indication of shock-accelerated CO gases associated with G109.1–1.0. On the other hand, IC 443 is known to exhibit shock-accelerated CO gases (DeNoyer 1979; Huang, Dickman, and Snell 1986; White *et al.* 1987). On what condition might shock-accelerated CO gases be observed? One might think that we cannot observe accelerated CO gases as shifted components in radial velocity because the motion of shocked gases on the surface of the main molecular cloud is perpendicular to the line of sight. However, positions C, D, and E of IC 443, which show shock-accelerated CO gases, are located just on the remnant shell (Huang, Dickman, and Snell 1986). Since the shocked gases are likely to be highly turbulent, the configuration of a shock front with respect to the line of sight is probably not important.

We suspect that the presence or lack of accelerated CO gases is explained in terms of difference in preshock density. It is likely that the peripheral part of the main molecular cloud mainly consists of atomic gases. We estimate the H_2 column density and the average H_2 density toward the peripheral part to be $<2 \times 10^{21} \text{ cm}^{-2}$ and $<20 \text{ cm}^{-3}$, respectively, by using the data of Tatematsu *et al.* (1987). Here we assume that the main molecular cloud has a depth along the line of sight of $\geq 30 \text{ pc}$, because the main molecular cloud has prevented an isotropic expansion of G109.1–1.0. The average density is much smaller than values observed toward typical molecular clouds ($\geq 10^2 \text{ cm}^{-3}$) (see, e.g., Myers 1978). Tatematsu *et al.* (1985) have shown that there is an H I cloud corresponding to the main molecular cloud. It seems that gas in the peripheral part of the main molecular cloud is mainly in atomic form, although a small amount of molecular gas is contained enabling us to observe it in CO. Shocked gas resulting from atom-rich preshock gas may consist mainly of atomic (or ionized) gas. The average densities in the two CO filaments are not large ($100\text{--}150 \text{ cm}^{-3}$ for the northern one and 30 cm^{-3} for the southern one), and we expect that these filaments also accompany atomic gas. If the two filaments are surrounded by atomic gas, the lack of accelerated CO gases in these filaments can be explained in the same way. On the other hand, the preshock H_2 density at position B in IC 443 was estimated to be $3000\text{--}3500 \text{ cm}^{-3}$ (Ziurys, Snell, and Dickman 1989) and is large enough to produce the shock-accelerated CO gas (see also discussion by Burton *et al.* 1988).

VI. SUMMARY

The supernova remnant G109.1–1.0 and the associated molecular cloud are studied through CO observations with the NRO 45 m radio telescope and the examination of archival X-ray data of the *Einstein Observatory*. The main results are summarized in the following two points.

(1) The CO arm extending from the main molecular cloud probably absorbs some of X-rays emitted from the remnant. The CO arm is resolved into two thin CO filaments. The anti-

correlation between these CO filaments and the X-ray intensity distribution of the remnant is generally good. The analysis of X-ray spectral data indicates that the spectrum toward the CO arm is harder than in the cloud-free direction. Together with the decrease of the X-ray intensity on the X-ray map, the harder X-ray spectrum toward the CO arm suggests the X-ray absorption by the CO arm. The absorbing column density toward the CO arm estimated from the X-ray analysis is compatible with the actual column densities of the two CO filaments estimated from the CO/¹³CO data of Tatematsu *et al.* (1987). However, we think that the true X-ray appearance of G109.1–1.0 is not much different from the observed one, because the X-ray absorption is a minor effect.

(2) We did not detect any broad CO emission which might

represent CO gas accelerated by G109.1–1.0. The upper bound to the intensity of shock-accelerated CO gas is 0.4 K for the whole region mapped in CO and 0.1 K toward 11 points observed with greater sensitivity. These upper bounds are below the intensity of 1–2 K of the accelerated CO gas observed toward IC 443.

We thank C. F. McKee for helpful comments and P. Mar-tinis for processing the X-ray spectra. This work was financially supported by the Grants-in-Aid for Scientific Research of the Ministry of Education, Science, and Culture, Japan (62420002, 63420003, 63611511, 63790144, and 63790145) and by NASA contract NAS8–30751. K. T. and T. I. are indebted to the Japan Society for the Promotion of Science.

REFERENCES

- Burton, M. G., Geballe, T. R., Brand, P. W. J. L., and Webster, A. S. 1988, *M.N.R.A.S.*, **231**, 617.
 Crampton, D., Georgelin, Y. M., and Georgelin, Y. P. 1978, *Astr. Ap.*, **66**, 1.
 DeNoyer, L. K. 1979, *Ap. J. (Letters)*, **232**, L165.
 DeNoyer, L. K., and Frerking, M. A. 1981, *Ap. J. (Letters)*, **246**, L37.
 Dickman, R. L. 1978, *Ap. J. Suppl.*, **37**, 407.
 Downes, A. 1983, *M.N.R.A.S.*, **203**, 695.
 Fahlman, G. G., and Gregory, P. C. 1981, *Nature*, **293**, 202.
 ———. 1983, in *IAU Symposium 101, Supernova Remnants and Their X-Ray Emission*, ed. J. Danziger and P. Gorenstein (Dordrecht: Reidel), p. 445.
 Giacconi, R., *et al.* 1979, *Ap. J.*, **230**, 540.
 Gregory, P. C., Braun, R., Fahlman, G. G., and Gull, S. F. 1983, in *IAU Symposium 101, Supernova Remnants and Their X-Ray Emission*, ed. J. Danziger and P. Gorenstein (Dordrecht: Reidel), p. 437.
 Gregory, P. C., and Fahlman, G. G. 1980, *Nature*, **287**, 805.
 ———. 1981, *Vistas Astr.*, **25**, 119.
 ———. 1983, in *IAU Symposium 101, Supernova Remnants and Their X-Ray Emission*, ed. J. Danziger and P. Gorenstein (Dordrecht: Reidel), p. 429.
 Heydari-Malayeri, M., Kahane, C., and Lucas, R. 1981, *Nature*, **293**, 549.
 Huang, Y.-L., Dickman, R. L., and Snell, R. L. 1986, *Ap. J. (Letters)*, **302**, L63.
 Hughes, V. A., Harten, R. H., Costain, C. H., Nelson, L. A., and Viner, M. R. 1984, *Ap. J.*, **283**, 147.
 Israel, F. P. 1980, *A.J.*, **85**, 1612.
 Koyama, K., Hoshi, R., and Nagase, F. 1987, *Pub. Astr. Soc. Japan*, **39**, 801.
 Kutner, M. L., and Ulich, B. L. 1981, *Ap. J.*, **250**, 341.
 Lampton, M., Margon, B., and Bowyer, S. 1976, *Ap. J.*, **208**, 177.
 Leahy, D. A., Venkatesan, D., Long, K. S., and Naranan, S. 1985, *Ap. J.*, **294**, 183.
 Myers, P. C. 1978, *Ap. J.*, **225**, 380.
 Raymond, J. C., and Smith, B. W. 1977, *Ap. J. Suppl.*, **35**, 419.
 Seward, F., Grindlay, J., Seaquist, E., and Gilmore, W. 1980, *Nature*, **287**, 806.
 Sofue, Y., Takahara, F., and Hirabayashi, H. 1983, *Pub. Astr. Soc. Japan*, **35**, 447.
 Tatematsu, K., Fukui, Y., Nakano, M., Kogure, T., Ogawa, H., and Kawabata, K. 1987, *Astr. Ap.*, **184**, 279.
 Tatematsu, K., Nakano, M., Yoshida, S., Wiramihardja, S. D., and Kogure, T. 1985, *Pub. Astr. Soc. Japan*, **37**, 345.
 Watson, M. G., Willingale, R., Grindlay, J. E., and Seward, F. D. 1983, *Ap. J.*, **273**, 688.
 White, G. J., Rainey, R., Hayashi, S. S., and Kaifu, N. 1987, *Astr. Ap.*, **173**, 337.
 Ziurys, L. M., Snell, R. L., and Dickman, R. L. 1989, *Ap. J.*, **341**, 857.

YASUO FUKUI, TAKAHIRO IWATA, and KEN'ICHI TATEMATSU: Department of Astrophysics, Nagoya University, Chikusa-ku, Nagoya 464-01, Japan

MAKOTO NAKANO: Department of Earth Science, Faculty of Education, Oita University, Oita 870-11, Japan

FREDERICK D. SEWARD: Harvard-Smithsonian Center for Astrophysics, 60 Garden Street, Cambridge, MA 02138